Spectroscopy and isotope shifts of the $4s3d\ ^1D_2$–$4s5p\ ^1P_1$ repumping transition in magneto-optically trapped calcium atoms

U. Dammalapati,* I. Norris, C. Burrows, A. S. Arnold, and E. Riis†
SUPA, Department of Physics, University of Strathclyde, Glasgow G4 0NG, United Kingdom
(Received 6 November 2009; published 26 February 2010)

We investigate a repumping scheme for magneto-optically trapped calcium atoms. It is based on excitation of the $4s3d\,^1D_2$–$4s5p\,^1P_1$ transition at 672 nm with an extended cavity diode laser. The effect of the repumping is approximately a factor of three increase in trap lifetime and a doubling of the trapping efficiency from a Zeeman slowed thermal beam. Added to this, the 672-nm laser repumps atoms from an otherwise dark state to yield an overall increase in detected fluorescence signal from the magneto-optic trap (MOT) of more than an order of magnitude. Furthermore, we report isotope shift measurements of the 672-nm transition, for the first time, for four naturally occurring even isotopes. Using available charge radii data, the observed shifts, extending up to 4.3 GHz, display the expected linear dependence in a King plot analysis. The measured shifts are used to determine the isotope shifts of the remaining ^{41,43,46}Ca isotopes. These might be of interest where less abundant isotopes are used enabling isotope selective repumping, resulting in enhanced trapping and detection efficiencies.

DOI: 10.1103/PhysRevA.81.023424 PACS number(s): 37.10.De, 42.62.Fi, 32.10.Fn, 71.20.Dg

I. INTRODUCTION

Optical pumping to dark states or states otherwise unconnected with the main cooling transition is a ubiquitous phenomenon in laser cooling and trapping experiments, whether applied to neutral atoms or ions. Although it is useful for experiments where a polarized sample is required, it is generally a limiting factor for the lifetime of a magneto-optical trap (MOT) and hence for the overall atom number and also the density that can be obtained.

For alkali-metal atoms, widely used in laser cooling and trapping experiments, it was realized early on that with only one cooling laser atoms will soon be optically pumped into the unconnected ground-state hyperfine level and lost from the cooling cycle. However, they can easily be "repumped" back into the cooling cycle using a separate laser operating a few GHz away or indeed by shifting the frequency of part of the main cooling laser using an electro-optic modulator (EOM) or an acousto-optic modulator (AOM) [1].

In general, repumping is more complicated and crucially depends on the subtle details of the particular atomic structure. The alkaline earth metal elements, for instance, have a $ns^2\ ^1S_0$–$nsnp\ ^1P_1$ main cooling transition but decays are allowed from the upper level of this transition to metastable D states and subsequently triplet P states. The branching ratios to these states are approximately 1:100 000 for Ca [2], 1:51300 for Sr [3], and 1:330 for Ba [4]. In the cases of Ca and Sr the branching to the metastable D states is sufficiently weak that it is not a limitation to achieve laser cooling although it does limit the MOT lifetime to a few tens of ms. In contrast, laser cooling of Ba is not possible without repumping.

For experiments where a short MOT lifetime results in an insufficient atom number, schemes will have to be implemented where additional lasers are used to repump the "lost" atoms back into the cooling cycle. The Ca energy levels relevant for the present work are shown in Fig. 1. The upper level of the strong 423-nm $4s^2\ ^1S_0$–$4s4p\ ^1P_1$ cooling transition has a weak decay to the singlet $4s3d\ ^1D_2$ state. From here the atoms decay, to the $4s4p\ ^3P_1$ state (78%), to the $4s4p\ ^3P_2$ state (22%), and to the $^1S_0$ ground state directly with a negligible decay rate [5]. Atoms that branch out to the $^3P_1$ state subsequently rejoin the cooling process if sufficiently large trap beams (>1 cm) are used [6]. Hence, the main "loss" is to the $^3P_2$ state, whose lifetime is about 118 min [7].

As most of the atoms end up in the metastable $^3P_2$ state, they can be repumped back to the ground state either by driving them to higher P states or back to the $^1D_2$ state. The former method was used by the Hamburg group employing a frequency doubled 860-nm diode laser [6] and the latter by our group using a 1530.5-nm distributed feedback laser [8].

Additional lasers have also been employed to reduce the atom temperature below the Doppler limit. Using the $^3P_2$ atoms for a second stage MOT on a 2-μm $^3P_2$–$^3D_3$ transition the Hamburg group [9] has achieved temperatures of about 100 μK as well as an increase in atom number. Temperatures as low as a few μK have been demonstrated using the narrow 657-nm $^1S_0$–$^3P_1$ intercombination line as a second cooling stage [10,11]. This is only possible by artificially shortening the $^3P_1$ lifetime using a quench laser coupling back to higher lying singlet states.

The lifetime of the MOT can also be extended and hence the number of trapped atoms increased by intercepting the leak out of the cooling cycle while the atoms are still in the $4s3d\ ^1D_2$ state. This is achieved by using a repump laser at the convenient wavelength of 672 nm to drive the atoms to the higher $4s5p\ ^1P_1$ state, from which a fraction of them will decay to the ground state through various states (Fig. 1). This was first demonstrated by the National Institute of Standards and Technology (NIST) group [12] and subsequently used by other groups [6,13–15]. In this article we investigate this repumping transition and show from a rate equation analysis that the observed order-of-magnitude increase in MOT fluorescence is a result of an increased MOT lifetime determined by the particular atomic decay rates combined with a more efficient capture of atoms into the trap and a clearing of a dark state.

*Present address: Kernfysisch Versneller Instituut, University of Groningen, Zernikelaan 25, 9747 AA Groningen, The Netherlands.
†e.riis@strath.ac.uk

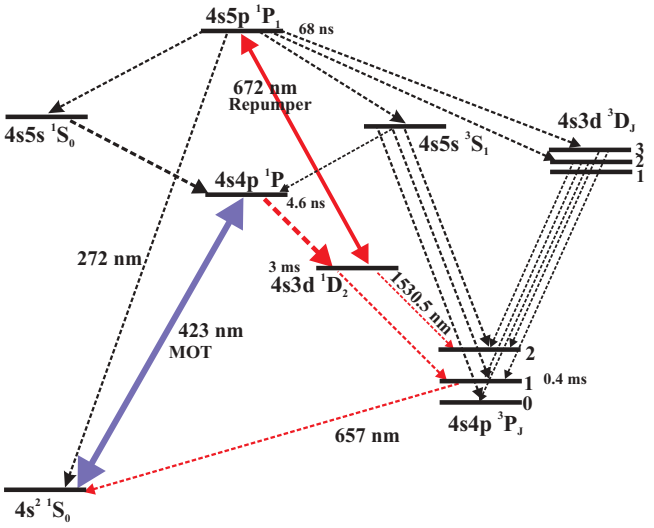

FIG. 1. (Color online) Low energy level diagram of the calcium atom with wavelengths and lifetimes of the states relevant for the current work. The transition rates along with their wavelengths of other contributing transitions are given in Table I. The solid arrows correspond to the $^1S_0$–$^1P_1$ 423-nm transition and to the 672-nm repump transition. The dashed arrows show the decays from the $4s4p\ ^1P_1$ state of the 423-nm MOT and various decay paths of the atoms from the $4s5p\ ^1P_1$ state to the low-lying states.

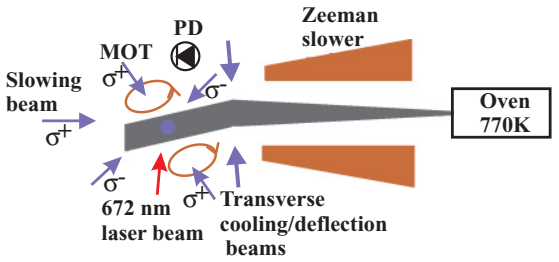

FIG. 2. (Color online) Experimental setup of the magneto-optical trapped calcium atoms used for the spectroscopy of the $4s3d\ ^1D_2$–$4s5p\ ^1P_1$ 672-nm transition. A thermal beam of atoms is slowed down using a Zeeman slower. The slowed atoms are transversely cooled and deflected using deflection laser beams to magneto-optic trap. The magnetic coils are shown in the figure. The fluorescence from the trapped atoms is detected with a photodiode (PD). The 672-nm laser beam is also shown.

Although the main isotope of Ca (^{40}Ca with a 96.941% abundance) is generally used in experiments such as optical frequency standards [12] and more recently the realization of quantum degeneracy [16], other even isotopes could be of interest for cold collision studies and the observation of optical Feshbach resonances [17]. The isotope ^{41}Ca with a half-life of 1.03×10^5 years can be used for radio-calcium dating and as a tracer for biomedical applications in the treatment of osteoporosis [18,19]. Atom trap trace analysis using laser cooling and trapping of neutral atoms has been developed and implemented for ultrasensitive analysis of various rare isotopes [20]. Detection of ^{41}Ca in a natural calcium sample is more challenging because its abundance ratio (^{41}Ca/Ca) is in the range 10^{-14}–10^{-15} [14,15]. The order-of-magnitude increase in MOT signal afforded by the 672-nm repumping scheme would provide a welcome increase in sensitivity for this type of measurement, enabling accurate knowledge of the isotope shift for this transition. Based on isotope shift measurements of the $4s3d\ ^1D_2$–$4s5p\ ^1P_1$ transition for the more abundant even isotopes we obtain a predicted value for the frequency required to repump the ^{41}Ca isotope as well as two other low abundance isotopes.

II. EXPERIMENTAL SETUP AND METHOD

Our experimental setup is shown schematically in Fig. 2. A detailed description of the apparatus and characterization of the 423-nm MOT was reported elsewhere [23]. An oven filled with high purity natural calcium is resistively heated to 500°C to produce a thermal beam. The atoms are decelerated by a counter-propagating laser beam in a 140-mm-long Zeeman slower. Atoms with initial velocities in the range 200–500 m/s are slowed to approximately 70 m/s, transversely cooled in a two-dimensional optical molasses stage and deflected toward the MOT. The optical molasses and MOT laser beams are 23 MHz red-detuned from the atomic resonance. The deflected atoms are confined in a MOT having an on-axis magnetic field gradient of 32 G/cm. The 423-nm fluorescence from the MOT is imaged with a lens system on to a calibrated and amplified photodiode. The number of trapped calcium atoms is typically around 10^6 for a pure ^{40}Ca MOT.

The blue laser light for the MOT is generated by a frequency doubled Ti:sapphire laser operating at 846 nm. More than 100 mW of light is generated using a periodically poled $KTiOPO_4$ (ppKTP), nonlinear, frequency doubling crystal in an external enhancement cavity [24]. For spectroscopic studies of the 672-nm transition the Ti:sapphire laser is frequency stabilized using the method described in Ref. [25].

Our previous work demonstrated MOT lifetimes of up to a few tens of ms consistent with the main loss mechanism being the decay of the atoms through the $4s3d\ ^1D_2$ state to the $4s4p\ ^3P_2$ state.

The 672-nm laser used for intercepting this decay is a semiconductor laser diode in an extended cavity configuration similar to the one described in Ref. [26]. The nominally 130-mW, 660-nm laser diode (HL6545MG) provides about 40 mW of usable power at 672 nm after heating it to 55°C. A portion of the light is coupled into a single mode polarization maintaining fiber and is used for frequency stabilization and calibration. The remaining 20 mW of laser light is available for the experiment and collimated to a beam with a ($1/e^2$) beam diameter of 10 mm. The transition has a saturation intensity of 1.0 mW/cm^2 allowing for strong saturation. However, it is worth noting that it is a $J = 2 \rightarrow 1$ transition and hence optical pumping into dark states is expected to play a significant role reducing the effective pumping rate. The state of polarization of the laser beam as it enters the vacuum chamber as well as that of the optional retroreflected beam can be controlled by the insertion of quarter-wave plates before and after the chamber.

For the repumping experiments the light sent through the optical fiber mentioned above is used for stabilizing the 672-nm laser frequency relatively to a stable HeNe laser using a transfer cavity method. The optical layout and setup is shown

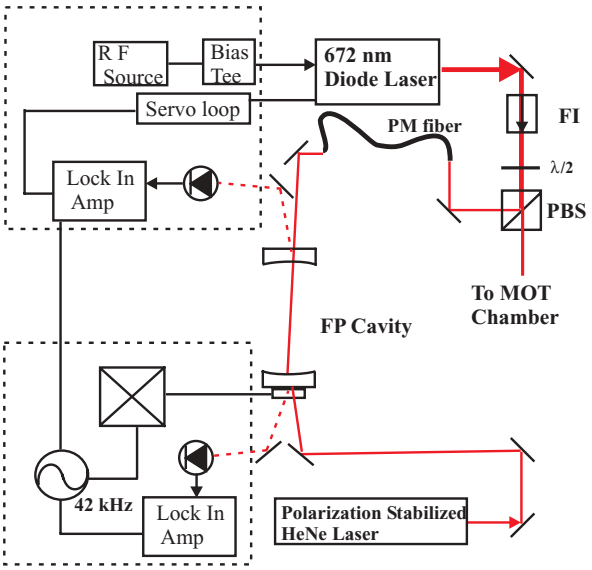

FIG. 3. (Color online) The schematic layout of the 672-nm laser frequency stabilization scheme. A 300-MHz free spectral range Fabry-Perot (FP) cavity of finesse 300 is used as a transfer cavity for frequency stabilization of the 672-nm laser. Details of the frequency stabilization method are given in the text.

in Fig. 3. This method is chosen over using another calcium or molecular transition because of its robustness and simplicity. Stabilization to the calcium $^1D_2$–$^1P_1$ transition is cumbersome as it requires a discharge-heat pipe oven in a buffer gas to sufficiently populate the $4s3d\ ^1D_2$ state [27,28]. Another option is to use the iodine (I_2) molecule, which provides frequency references throughout the visible and near infrared (IR). The nearest line is 566 MHz red shifted from the calcium 672-nm transition. However, in order to get a sufficient signal to noise ratio the iodine cell would have to be heated to more than 400°C.

The central part of our frequency stabilization system is a 300-MHz free spectral range confocal Fabry-Perot interferometer with a finesse of approximately 300. A transmission fringe of this cavity is locked to the HeNe laser. If we now merely locked the 672-nm diode laser to the cavity we would not necessarily hit the Ca resonance, so we have to introduce a variable offset to allow us to tune between the cavity transmission modes. This is achieved by applying a radio frequency modulation to the diode drive current through a bias-tee and locking one of the resulting sidebands to the cavity [29]. A typical operating condition for the experiment is a modulation frequency of 50–70 MHz at a power level of −2 dBm. This results in approximately 10% of the laser power in each first-order sideband. The chosen sideband remains locked to the cavity as the modulation frequency is varied by tens of MHz and the carrier consequently tunes across the Ca resonance.

The HeNe laser is a standard two-mode internal-mirror-type laser with successive oscillating modes that are linearly polarized but orthogonal to each other. The cavity length is stabilized using thermal feedback to a fixed ratio of the power in the two orthogonal polarizations [30]. This laser remains locked indefinitely with frequency fluctuations in the range of a few MHz. Appropriate electronic error signals for stabilizing the cavity to the HeNe laser and the diode laser to the cavity are obtained by modulating the cavity length at a frequency of 42 kHz (modulation amplitude of 1 MHz) and demodulating the respective laser transmissions with lock-in amplifiers.

III. MOT REPUMPING

Examples of the loading curves of the 423-nm $^1S_0$–$^1P_1$ MOT are shown in Fig. 4(A) with and without the resonant 672-nm repump laser. This data shows a factor of 12 increase in the 423-nm fluorescence signal and a factor of 2.9 increase in the trap lifetime in the presence of the repump laser and illustrates several key aspects of the system. First of all, the lifetime with the repumper is about 47 ms, which is still shorter than what would be expected from collision of the trapped atoms

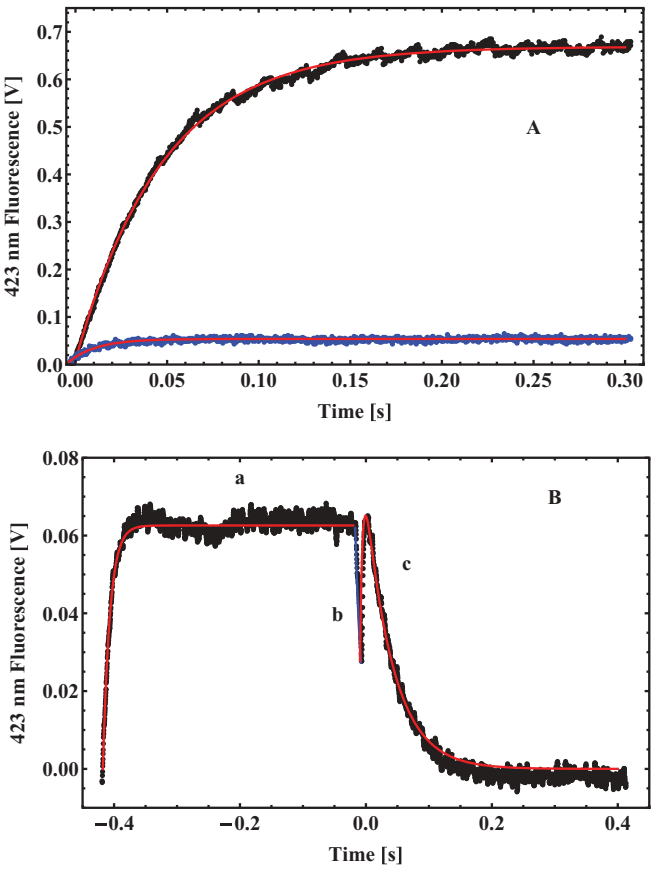

FIG. 4. (Color online) (A) Loading of the 423-nm $^1S_0$–$^1P_1$ MOT with (upper) and without (lower) the resonant frequency stabilized 672-nm laser. The smooth curves are exponential fits to the data. (B) 423-nm MOT fluorescence in the absence and subsequent presence of the 672-nm repumper. (a) The MOT (lifetime 16 ms) is loaded for 400 ms after which filling is terminated by extinguishing the deflection laser beams after the Zeeman slower. (b) Decay of the 423-nm MOT (lifetime 16 ms) is allowed for 20 ms, which is larger than the transit time from the deflection region to the MOT. This ensures no further atoms are being loaded. (c) The 672-nm laser is switched on for 400 ms. The initial rise (with a time constant of 400 ms) is due to the atoms previously shelved in the $^1D_2$ state. The subsequent decay shows the increased lifetime of 43 ms for the repumped MOT. Curves a and b [Eq. (1)], and curve c [Eq. (2)] are the fits to the data.

TABLE I. Transition rates (A_{ik}) and vacuum wavelengths (λ) from low-lying states in calcium.

Upper level	Lower level	A_{ik} (10^7 s^{-1})	λ (nm)
$4s5p\,^1P_1$	$4s5s\,^1S_0$	0.2126	2928.81[a]
	$4s5s\,^3S_1$	0.01399	1926.00[a]
	$4s3d\,^3D_1$	0.01053	609.89[a]
	$4s3d\,^3D_2$	0.009349	610.41[a]
	$4s3d\,^1D_2$	1.209	671.954[b]
	$4s^2\,^1S_0$	0.02674	272.2[b]
$4s5s\,^1S_0$	$4s4p\,^1P_1$	2.435	1034.66[a]
$4s5s\,^3S_1$	$4s4p\,^1P_1$	0.00001465	1267.8[a]
	$4s4p\,^3P_0$	0.96	610.441[b]
	$4s4p\,^3P_1$	2.87	612.391[b]
	$4s4p\,^3P_2$	4.77	616.388[b]
$4s3d\,^3D_1$	$4s4p\,^3P_0$	0.02149	1931.4494[a]
	$4s4p\,^3P_1$	0.01565	1951.1064[a]
	$4s4p\,^3P_2$	0.0009779	1992.2632[a]
$4s3d\,^3D_2$	$4s4p\,^3P_1$	0.02838	1945.2893[a]
	4s4p $^3P_2$	0.008869	1986.7614[a]

[a]Data from Ref. [21].
[b]Data from Ref. [22].

with background gas and losses due to the inelastic two-body collisions between cold calcium atoms [16]. The reason for this is that the 672-nm transition is not an ideal repump transition. Based on the published values for the relevant decay rates summarized in Table I we find that 81.5% of the atoms excited by the laser decay back on the same transition. Apart from its tendency to increase the rate of pumping into dark states this in itself is not a problem for the actual repumping but merely results in an increased laser power requirement. Most of the rest of the atoms return to the ground state via the $4s5s\,^1S_0$ and $4s4p\,^1P_1$ levels providing the desired repumping. However, a small fraction decays to the triplet scheme, where approximately 50% end up in the long-lived $^3P_2$ and $^3P_0$ states and are lost from the cooling cycle. This represents an overall loss of about 1.2% from the repumping cycle compared with 17.3% being successfully repumped. Thus, the repumping reduces an atom's chance of being lost from the 423-nm MOT cooling cycle from the 22% due to the $4s3d\,^1D_2$ branching ratio to the $^3P_2$ state to 7%. This intuitive and approximate result also follows from a rigorous solution of the time-dependent rate equations for the system as detailed in Sec. III A.

Secondly, the 423-nm MOT fluorescence increases in the presence of the repump laser as atoms shelved in the $^1D_2$ state are brought back into the cooling cycle. As seen in Fig. 4(B) we have recorded the 423-nm fluorescence as the repumper is switched on and in the absence of further loading of the MOT. Using a detection system with a response time of <0.1 ms and for the typical operating conditions for the experiment we see an approximate doubling of the fluorescence on a timescale of 0.4 ms. The data shown in Fig. 4(B) are fitted with the three functions given in Eqs. (1) and (2):

$$N(t) = N_0[1 - \exp(-t/\tau_1)] \quad t < t_0, \tag{1a}$$

$$N(t) = N_0 \exp[-(t - t_0)/\tau_1] \quad t_0 < t < t_r, \tag{1b}$$

where τ_1 is the loading and decay time for the 423-nm MOT. The loading takes place between $t = 0$ and $t = t_0$. The repumping laser is switched on at $t = t_r$ slightly after the filling has stopped to ensure that no new atoms are captured. The fluorescence signal now follows a more complicated expression given by the solution to the differential equation:

$$\dot{N}(t) = N_d \exp[-(t - t_r)/\tau_r]/\tau_r - N(t)/\tau_2 \quad t > t_r, \tag{2}$$

where the first term represents atoms previously in the $^1D_2$ state and brought into the cooling cycle by the repumper and the second represents the decay (time constant τ_2) of the MOT in the presence of the 672-nm repump laser. N_d is the initial number of atoms in the $^1D_2$ state and $1/\tau_r$ the rate of repumping.

The magnitude of the increase seen in Fig. 4(B) agrees well with steady-state rate equation solutions indicating that approximately half the population resides in the $^1D_2$ state in the absence of the repumper. The timescale for bringing these atoms back to the ground state (400 μs) confirms the importance of optical pumping into dark states on the repump transition. Assuming on resonant excitation at saturation we would expect a 672-nm excitation every third of a microsecond. If all $^1D_2$ sublevels were driven at this rate repumping requiring on average six scattering events would only take a couple of microseconds in stark contrast with the observed rate.

Finally we note that the steady-state number of atoms in the MOT is the product of the filling rate into the MOT and the MOT lifetime. Taking the increased signal due to the repumped $^1D_2$ atoms into account we observe an atom number increase of about a factor of six. This is roughly twice what is expected from the increased lifetime and suggests that the capture rate of atoms from the slowed atomic beam is also improved by the presence of the 672-nm laser.

This beneficial effect of the repumper on the filling rate was not expected. Repumping is generally seen as unnecessary for the Zeeman slower as the 1:100 000 loss into the $^1D_2$ state is insignificant as an atom scatters of order 20×10^3 photons to slow from an initial velocity of order 500 m/s to near rest. However, the strongly over-damped nature of the MOT means that an atom spends much longer than this (a few ms) being fully captured into the center of the MOT. We have modeled this process numerically for a hypothetical closed cooling transition and find that for our experimental conditions most atoms would scatter between 5×10^4 and 1×10^5 photons in this final stage of the trapping. Thus, for the real atomic system, there is now a significant probability of decaying into the $^1D_2$ state. About three quarters of these atoms will return to the ground state after approximately 3.5 ms. For atoms near the MOT center this is not a problem as they are slow enough not to travel outside the MOT region in this time [6]. However, due to the strong damping of the cooling beams, atoms approaching the MOT center travel with a velocity such that the Doppler shift approximately equals the local Zeeman shift. This corresponds to 0.6 m s^{-1}/G, so atoms decaying to the $^1D_2$ state outside a 5-G contour will escape the MOT region before returning to the ground state. Thus, with the experimental 32-G/cm field gradient the majority of the region is outside this contour and atoms decaying to the $^1D_2$ state here will in general not be given a second chance of getting trapped. We can qualitatively understand the observed doubling of the filling rate in the presence of the repumper by

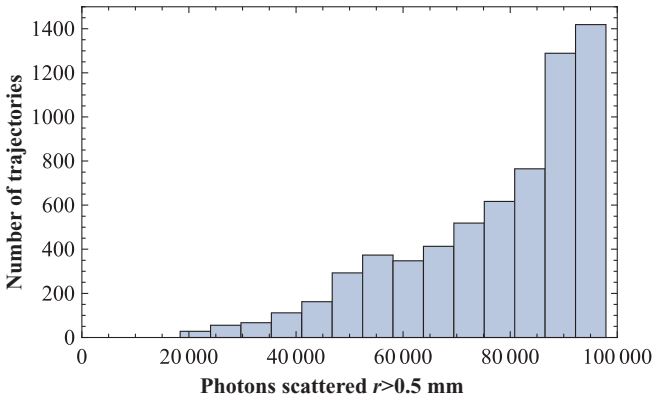

FIG. 5. (Color online) Histogram of the number of photons scattered by 6500 simulated deflected beam atoms until they are captured by the MOT (i.e., until they reach the MOT radius $r = 0.5$ mm). Experimental parameters were used for the three-dimensional classical trajectory simulation. Total photon scatter is estimated via the integral of the average local scattering rate over time. A fraction of 47% of the atoms never leave the cooling cycle.

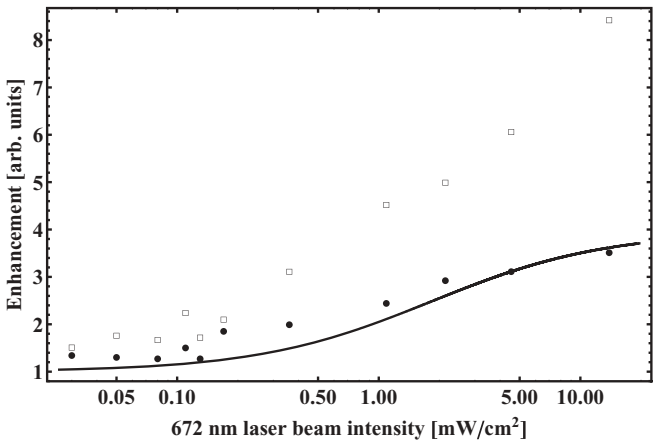

FIG. 6. Lifetime (●) of the $^1S_0$–$^1P_1$ MOT measured at different intensities of the 672-nm laser beam intensities. Increase in the 423-nm steady-state MOT fluorescence (□) as a function of the 672-nm laser beam intensity. In both cases the 423-nm MOT beams intensity is fixed. The solid curve is obtained from the rate equation model.

considering a typical atom scattering 8×10^4 photons before it is trapped (Fig. 5). With a 1:1 $\times$ 10^5 chance of getting lost for each excitation event the chance of actually ending up in the trap is therefore less than 50%. By introducing the 672-nm repumper we virtually eliminate the time spent in the $^1D_2$ state and only 1 in 15 of these atoms are lost. This roughly doubles the probability of surviving the 8×10^4 scattering events to more than 95%.

A. Rate equations

The loss mechanisms due to the atomic structure can be modeled using rate equations for the relevant atomic levels shown in Fig. 1. Based on the known values for the decay rates it is, however, possible to reduce this many-level system to an effective five-level system. Level 1, 2, and 3 are the ground state, $4s4p\ ^1P_1$ and $4s3d\ ^1D_2$ levels, respectively. Level 4 is the loss channel (i.e., primarily $^3P_2$ but also any population decaying to $^3P_0$ as well as a small fraction, ε, decaying to $^3P_1$ and escaping from the MOT volume before decaying to the ground state). The remaining $^3P_1$ population is represented by a direct decay from Level 3 to Level 1 with the smaller $^1D_2$–$^3P_1$ decay rate. Level 5 is the $4s5p\ ^1P_1$ level reached by the 672-nm laser. The decays from here are directly to Level 1, to Level 2 via $4s5s\ ^1S_0$ (represented by the smaller $4s5p$–$4s5s$ decay rate) and to the triplet scheme. Of the latter, a factor of 1–α (approximately half) is lost (i.e., a decay into Level 4) while the rest (a factor of α) effectively decays to the ground state.

$$\dot{N}_1 = R - L(\Delta, I)(N_1 - N_2) + \Gamma_{21}N_2 + (1-\varepsilon) \times \Gamma_{31}N_3 + (\Gamma_{51} + \alpha\Gamma_{54})N_5 \quad (3)$$

$$\dot{N}_2 = L(\Delta, I)(N_1 - N_2) - (\Gamma_{21} + \Gamma_{23})N_2 + \Gamma_{52}N_5 \quad (4)$$

$$\dot{N}_3 = \Gamma_{23}N_2 - (\Gamma_{31} + \Gamma_{34} + \Gamma_r)N_3 + (\Gamma_{53} + \Gamma_r)N_5 \quad (5)$$

$$\dot{N}_4 = (\Gamma_{34} + \varepsilon\Gamma_{31})N_3 + (1-\alpha)\Gamma_{54}N_5 \quad (6)$$

$$\dot{N}_5 = \Gamma_r(N_3 - N_5) - (\Gamma_{51} + \Gamma_{52} + \Gamma_{53} + \Gamma_{54})N_5, \quad (7)$$

where

$$L(\Delta, I) = \frac{s\Gamma_{12}}{2[1 + (2\Delta/\Gamma_{12})^2]}, \quad (8)$$

and $s = I/I_{\text{sat}}$ and I_{sat} is the saturation intensity of the $^1S_0$–$^1P_1$ transition. From the literature (see Table I), $\Gamma_{21} = 2.18 \times 10^8\ \text{s}^{-1}$; $\Gamma_{23} = 2180\ \text{s}^{-1}$; $\Gamma_{31} = 354\ \text{s}^{-1}$; $\Gamma_{34} = 96\ \text{s}^{-1}$; $\Gamma_{51} = 2.67 \times 10^5\ \text{s}^{-1}$; $\Gamma_{52} = 2.13 \times 10^6\ \text{s}^{-1}$; $\Gamma_{53} = 1.21 \times 10^7\ \text{s}^{-1}$; $\Gamma_{54} = 3.40 \times 10^5\ \text{s}^{-1}$. The parameter R represents the filling of atoms into the MOT. For typical experimental conditions $\varepsilon = 4.2$ % [23].

The equations can be solved analytically in steady state ($\dot{N}_1 = \dot{N}_2 = \dot{N}_3 = \dot{N}_5 = 0$) to determine the equilibrium populations. We have also solved the time-dependent equations numerically to determine the MOT lifetimes. We find that for typical 423-nm operating conditions and a 672-nm laser intensity well above saturation that the lifetime is increased by between a factor of 2.5 and 3.5, which is in good agreement with the experimental data shown in Fig. 6.

B. MOT lifetime and atom number

Measurements of the trap lifetime and increase in MOT fluorescence were carried out keeping the intensity of the 423-nm MOT beams constant at different intensities of the 672-nm laser beam (see Fig. 6). We observe almost no change in the 423-nm MOT lifetime at intensities well below the saturation intensity of 1 mW/cm^2 of the 672-nm transition while it triples at high intensities. The solid curve is obtained from solving the rate equations but in order to get this qualitative agreement with the data we have used a saturation intensity of 15 mW/cm^2. We again attribute that to the reduced efficiency of the repumping due to pumping into dark states on the 672-nm transition.

A quantitative understanding of this saturation effect is beyond the capabilities of our relatively simple rate equation analysis. A full treatment would have to include the individual magnetic sublevels and the dynamics of the atoms in the quadrupole magnetic field, so we shall here only outline some of the qualitative features of the process. First, we note that given the $4s5p\ ^1P_1$ branching ratios a group of stationary atoms illuminated by a single beam polarized along the magnetic field direction after scattering only a few photons each approach a

steady state of 78% of the atoms in the dark $m_j = 2$ states and 22% repumped. Thus, the repumping process is strongly impeded by the presence of the dark states. Secondly, one might expect that the inclusion of a retroreflected beam of different polarization would set up a sufficient polarization gradient that an atom, which, in this case, moves of order of half a wavelength per excitation time would see a sufficiently scrambled polarization, that pumping into the dark states was prevented. However, this was observed experimentally not to be the case. To understand this we have to consider the magnitude of the MOT magnetic field. For an on-axis gradient of 32 G/cm all atoms apart from the ones in the very center (radius of order 1 mm) see a Zeeman shift larger than the natural linewidth of the transition (1.1 MHz; both g factors are 1). Thus, the atoms effectively only interact with one beam and the pumping into the dark states prevail. Atomic motion into a region of different magnetic field direction would enable coupling into the dark states. For the expected atomic velocity of order 1 m/s the timescale for this is about 1 ms although a higher repump intensity would tend to shorten this. As seen in Fig. 4(B) we observe repumping time of about 0.4 ms. Thirdly, a high repump intensity would also expand the volume where the Zeeman shift is less than or comparable to the power broadened linewidth. For a 15 times increase in repump intensity we would expect an almost fourfold increase in linear dimension and thus approaching the entire MOT volume.

Also shown in Fig. 6 is the corresponding enhancement in the detected 423-nm fluorescence signal. It should be noted again, that this is the product of the contributions from the enhanced lifetime, the increased filling rate and the approximate doubling of the signal due to the repumping of the $^1D_2$ state. We note that the signal enhancement is less than a factor of two above the lifetime enhancement for most intensities apart from the highest. As we would expect the clearing of the $^1D_2$ state in trapped atoms to be reasonably effective even at moderate intensities this might indicate that the effect of the repumper on the filling rate only kicks in at high intensities.

We have also investigated the enhancement of lifetime with beam size for fixed peak intensity of 14 mW/cm^2. Figure 7 shows that the lifetime is only affected for beam diameters larger than 3 mm indicating the importance of the repumper in capturing escaping atoms. Also plotted in Fig. 7 is the enhancement of the ratio of MOT fluorescence to trap lifetime. This measure identifies the contributions from trapped atoms previously shelved in the $^1D_2$ state and the enhanced loading. It seems reasonable to assume that the former is responsible for the doubling of the signal at 3-mm beam diameter while the further doubling with increased beam size is due to the increased loading primarily required at larger distances from the MOT center.

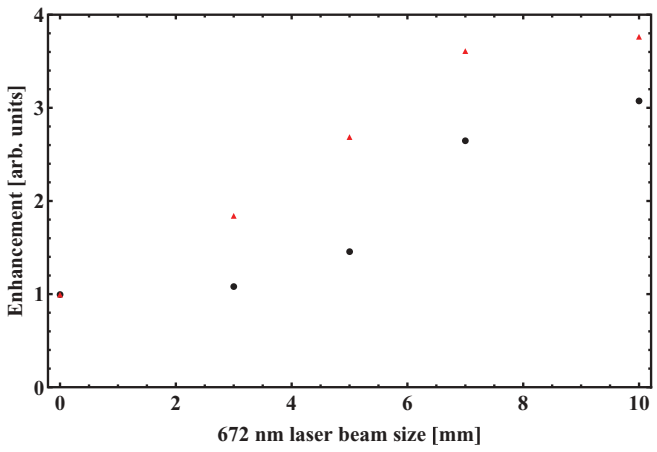

FIG. 7. (Color online) Enhancement of MOT parameters with increasing 672-nm laser beam diameter. MOT lifetime (●) and ratio of steady-state fluorescence to lifetime (▲). The intensity of the 672-nm laser is 14 mW/cm^2.

IV. ISOTOPE SHIFTS

The isotope shifts of a transition in an element have contribution from three components [31,32], which can be written as:

$$\delta\nu^{A_1A_2} = (M_{\mathrm{NMS}} + M_{\mathrm{SMS}})\frac{A_1 - A_2}{A_1A_2} + F_{\mathrm{FS}}\delta\langle r^2\rangle^{A_1A_2} \quad (9)$$

where $\delta\langle r^2\rangle^{A_1A_2}$ is the change in mean-square nuclear charge radii between two isotopes under investigation, A_1 and A_2 are the mass numbers of the isotopes in atomic mass units (here for calcium, $A_1 > A_2 = 40$), M_{NMS} is the normal mass-shift component, M_{SMS} is the specific mass-shift component, and F_{FS} is the field-shift component.

The normal mass shift can be calculated by the expression,

$$M_{\mathrm{NMS}} = \nu\frac{m_e}{m_p}, \quad (10)$$

where m_e is mass of the electron, m_p is the mass of the proton, and ν is the frequency of the transition. The normal mass shift of the 672-nm transition is 243.1 GHz. The specific mass shift and field shift are both characteristics of a particular atomic transition and can be derived from the measured isotope shifts. On the other hand the $\delta\langle r^2\rangle^{A_1A_2}$ are common to all transitions.

In general, the modified isotope shifts ($\Delta\nu_M^{A_1A_2}$) are used in the King plot analysis of the isotopes. It is obtained by subtracting the normal shifts from the experimentally measured isotope shifts and multiplying Eq. (9) by the quantity $A_1A_2/(A_1 - A_2)$ on both sides. It is then written as

$$\Delta\nu_M^{A_1A_2} = M_{\mathrm{SMS}} + F_{\mathrm{FS}}\delta\langle r^2\rangle^{A_1A_2}\frac{A_1A_2}{A_1 - A_2}, \quad (11)$$

where

$$\Delta\nu_M^{A_1A_2} = \delta\nu^{A_1A_2}\frac{A_1A_2}{A_1 - A_2} - M_{\mathrm{NMS}}. \quad (12)$$

A. Method and results

The isotope shift measurements are carried out by scanning the diode laser across the 672-nm transition and simultaneously recording the MOT signal and the transmission fringes of a high-finesse Fabry-Perot cavity. This cavity acts to calibrate the laser scan and as a stable reference allowing frequency differences to be measured from separate scans of different isotopes. The cavity consists of a flat mirror and a mirror with radius of curvature $R = 500$ mm. Both are coated with high-reflectivity coatings giving a finesse in excess of 1×10^5. The mirrors are separated by an approximately

100-mm-long ultralow expansion (ULE) glass spacer and the cavity is placed inside a vacuum chamber maintained at a pressure of 3.9×10^{-9} mbar. The cavity free spectral range is 1498.9(6)MHz. However, the input light to the cavity is deliberately misaligned allowing us to also record higher order transverse modes. These are spaced by 238.5(1) MHz thus providing a finer scale for the calibration of the laser scan.

A scan is typically 3.5 GHz limited by the piezo tilting the grating in the laser. This is sufficient to cover three isotopes (for detecting the farthest away ^{48}Ca isotope the 672-nm laser frequency is shifted such that the isotopes 44 and 48 can be detected in a single scan). While the 672-nm diode laser scans continually the Ti:sapphire laser frequency is scanned slowly detecting individual isotopes as an increase in the fluorescence of the 423-nm MOT when both lasers are resonant with the isotope's transitions.

The isotope shifts are derived making use of the individual isotope scan and its corresponding transmission spectrum of the FP cavity. The position in scan time for each of 15–20 transmission peaks is fitted and its frequency determined by its mode number identification. A fourth-order polynomial fit is then used to represent the laser frequency as a function of time for each individual scan allowing interpolation between cavity transmission peaks. This effectively allows us to compensate for the nonlinearity of the scan on the hundreds of MHz scale and convert the raw signal versus scan time data into signal versus frequency. The accuracy of this conversion is limited by the linewidth of the laser (5 MHz) and frequency jitter as observed with the high-finesse cavity (linewidth about 100 kHz). We can generally determine the position of the transmission peaks to better than 1 MHz but frequency jitter of up to a few MHz is observed. The uncertainty in the determination of the Ca resonance peak position is less than 1 MHz (less than 1% of the resonance width). The combined uncertainties given in Table II for the measured isotope shifts are obtained from the weighted average of the individual spectral scans.

The measured isotope shifts of the four even isotopes of calcium in the $4s3d\ ^1D_2$–$4s5p\ ^1P_1$ transition are given in Table II. Typical spectra of some of the observed isotopes are shown in Fig. 8. All the data were fitted with Lorentzian functions with independent width. The observed linewidths were 80–90 MHz with contributions from laser linewidth, saturation and Zeeman shift in the MOT field.

TABLE II. Measured isotope shifts of calcium for the $4s3d\ ^1D_2$–$4s5p\ ^1P_1$ transition. All the values are in MHz. The values shown in parentheses are errors. Values given with an $*$ are the estimated centroids of the remaining three isotopes.

Isotope pair	Isotope shift (MHz)
40–42	1181(3)
40–44	2268(3)
40–48	4239(9)
42–44	1087(4)
44–48	1971(9)
40–41	620(1)*
40–43	1755(2)*
40–46	3298(3)*

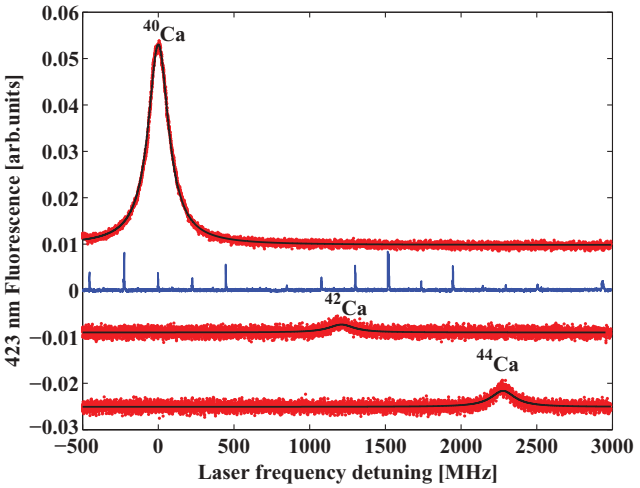

FIG. 8. (Color online) The ^{42,44}Ca isotope spectra with respect to the 672-nm laser frequency detuning of the ^{40}Ca isotope. The ^{48}Ca isotope spectrum is not shown. All the isotopes are detected as an increase in the $^1S_0$–$^1P_1$ MOT fluorescence when the 423-nm laser is tuned to the resonance of the respective isotope. The black curves are Lorentzian fits. The measured linewidths are 80–90 MHz. A typical mode spectrum of the high-finesse Fabry-Perot cavity used for calibration of the frequency axis is also shown. Offsets to the isotope data are added to distinguish the isotope positions for clarity.

As indicated by Eq. (11) the measured modified isotope shifts are expected to depend linearly on the mean-square charge radius $\delta\langle r^2\rangle^{A_1A_2}$. Values for the latter are derived from the available vast experimental data and obtained from Ref. [33]. The resulting King plot is shown in Fig. 9. From the linear fit to the data we obtain a specific mass shift of

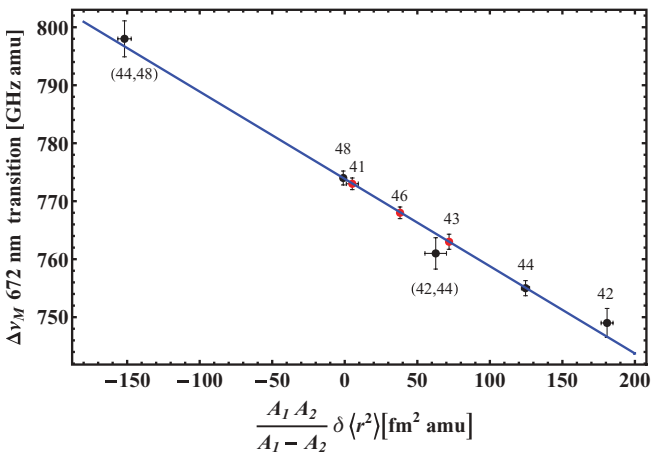

FIG. 9. (Color online) King plot for the 672-nm repump transition. The modified isotope shifts ($\Delta\nu_M^{A_1A_2}$) are plotted against the modified difference in root mean square (RMS) nuclear charge radii ($\frac{A_1A_2}{A_1-A_2}\delta\langle r^2\rangle^{A_1A_2}$) of the calcium isotopes. The specific mass shift M_{SMS} and the field shift F_{FS} of the $4s3d\ ^1D_2$–$4s5p\ ^1P_1$ transition at 672 nm are determined from a linear regression analysis, which is shown as a solid line. The points relating to the 42, 44, and 48 are the experimental data while those relating to isotopes 41, 43, and 46 are the estimated center of gravities.

$M_{\mathrm{SMS}} = 774.0(0.7)$ GHz a.m.u. and field shift component $F_{\mathrm{FS}} = -149.3(7.1)$ MHz/fm^2. The close fit to the data points validates the nuclear charge radii data and isotope shift data of this work.

Given the operating limits for the calcium oven, the less abundant isotopes ^{43}Ca (0.135%) with nuclear spin ($I = 7/2$) and ^{46}Ca (0.004%) ($I = 0$) could not be observed with the current detection system based on recording the fluorescence from the $^1S_0$–$^1P_1$ transition. The positions of the centroids of all the unobserved isotopes ^{41,43,46}Ca relative to ^{40}Ca, however, can be estimated using Eqs. (11) and (12) from the measured isotope shifts of the abundant even isotopes and from known difference in root mean-square charge radii $\delta\langle r^2\rangle^{A_1A_2}$ of the isotopes [33]. The determined isotope shift values and their estimated errors in the parentheses are given in Table II with an asterisk. As shown by Moore *et al.* [14], the hyperfine structure for the odd isotopes is also a limiting factor for effective repumping. To a large extent, though, this can be solved by broadening the spectrum of the laser [1].

The specific mass shift for the $4s3d\ ^1D_2$–$4s5p\ ^1P_1$ transition is noticeably different from that of the $4s^2\ ^1S_0$–$4s4p\ ^1P_1$ transition. The SMS is larger than the NMS [$M_{\mathrm{SMS}}/M_{\mathrm{NMS}} = 3.183(3)$] and has a positive sign for the D–P transition whereas the SMS is very small and has a negative sign to the NMS in the S–P transition ($M_{\mathrm{SMS}}/M_{\mathrm{NMS}} = -0.0680(3)$) [34]. The SMS is known to be much higher in lighter elements in transitions that change the number of "d" electrons compared to the "s" and "p" electrons involved transitions [32].

V. CONCLUSION

To summarize, we have reported the spectroscopy of the 672-nm $4s3d\ ^1D_2$–$4s5p\ ^1P_1$ transition and isotope shifts of four even isotopes of calcium. We observe about a factor of 12 increase in the fluorescence signal from a 423-nm MOT when the 672-nm laser beam is used. This is a result of three contributions: a tripling of the MOT lifetime, a doubling of efficiency with which atoms are captured into the MOT, and finally a factor of two increase as atoms previously shelved in the $^1D_2$ state join the cooling cycle. We have investigated the dependence of the MOT lifetime on the 672-nm laser intensity and recorded an increase of up to a factor of 3.5. Good agreement with an analytical model is obtained when taking into account that the repumping laser will transfer atoms into dark magnetic sublevels.

The isotope shifts were measured for the four most abundant even calcium isotopes. From these measurements we are able to predict the transition frequencies for the remaining long-lived isotopes. This is of relevance for situations where the less abundant isotopes are being trapped. In addition to the order of magnitude increase in MOT signal the isotope selective repumping provides additional discrimination against the majority isotopes.

ACKNOWLEDGMENTS

This work was supported by the United Kingdom Engineering and Physical Sciences Research Council (EPSRC).

[1] C. S. Adams and E. Riis, Prog. Quantum Electron. **21**, 1 (1997).
[2] N. Beverini, F. Giammanco, E. Maccioni, F. Strumia, and G. Vissani, J. Opt. Soc. Am. B **6**, 2188 (1989).
[3] X. Xu, T. H. Loftus, J. L. Hall, A. Gallagher, and J. Ye, J. Opt. Soc. Am. B **20**, 968 (2003).
[4] U. Dammalapati, S. De, K. Jungmann, and L. Willmann, Eur. J. Phys. D **53**, 1 (2009).
[5] N. Beverini, E. Maccioni, F. Sorrentino, V. Baraulia, and M. Coca, Eur. J. Phys. D **23**, 223 (2003).
[6] J. Grünert and A. Hemmerich, Appl. Phys. B **73**, 815 (2001).
[7] A. Derevianko, Phys. Rev. Lett. **87**, 023002 (2001).
[8] U. Dammalapati, I. Norris, C. Burrows, and E. Riis (manuscript in preparation).
[9] J. Grünert and A. Hemmerich, Phys. Rev. A **65**, 041401(R) (2002).
[10] E. A. Curtis, C. W. Oates, and L. Hollberg, Phys. Rev. A **64**, 031403(R) (2001).
[11] T. Binnewies, G. Wilpers, U. Sterr, F. Riehle, J. Helmcke, T. E. Mehlstaüber, E. M. Rasel, and W. Ertmer, Phys. Rev. Lett. **87**, 123002 (2001).
[12] C. W. Oates, F. Bondu, R. W. Fox, and L. Hollberg, Eur. J. Phys. D **7**, 449 (1999).
[13] C. Degenhardt, T. Binnewies, G. Wilpers, U. Sterr, F. Riehle, C. Lisdat, and E. Tiemann, Phys. Rev. A **67**, 043408 (2003).
[14] I. D. Moore, K. Bailey, J. Greene, Z. T. Lu, P. Müller, T. P. O'Connor, C. Geppert, K. D. A. Wendt, and L. Young, Phys. Rev. Lett. **92**, 153002 (2004).
[15] S. Hoekstra, A. K. Mollema, R. Morgenstern, H. W. Wilschut, and R. Hoekstra, Phys. Rev. A **71**, 023409 (2005).
[16] S. Kraft, E. Vogt, O. Appel, F. Riehle, and U. Sterr, Phys. Rev. Lett. **103**, 130401 (2009).
[17] R. Ciurylo, E. Tiesinga, and P. S. Julienne, Phys. Rev. A **71**, 030701(R) (2005).
[18] G. M. Raisbeck and F. Yiou, Nature **277**, 42 (1979).
[19] D. Elmore, M. H. Bhattacharyya, N. Sacco-Gibson, and D. P. Peterson, Nucl. Instrum. Methods Phys. Res. B **52**, 531 (1990).
[20] C. Y. Chen, Y. M. Li, K. Bailey, T. P. O'Connor, L. Young, and Z. T. Lu, Science **286**, 1139 (2004).
[21] R. L. Kurucz and B. Bell, 1995 Atomic Line Data, Kurucz CD-ROM No. 23, Smithsonian Astrophysical Observatory, Cambridge, MA, 1995.
[22] Y. Ralchenko, A. E. Kramida, and J. Reader (NIST ASD team), NIST Atomic Spectra Database, 2008.
[23] U. Dammalapati, I. Norris, L. Maguire, M. Borkowski, and E. Riis, Meas. Sci. Technol. **20**, 095303 (2009).
[24] F. Torabi-Goudarzi and E. Riis, Opt. Commun. **227**, 389 (2003).
[25] U. Dammalapati, I. Norris, and E. Riis, J. Phys. B: At. Mol. Opt. Phys. **42**, 165001 (2009).
[26] A. Arnold, J. S. Wilson, and M. Boshier, Rev. Sci. Instrum. **69**, 1236 (1998).
[27] R. L. Cavasso-Filho, A. Mirage, A. Scalabrin, D. Pereira, and F. C. Cruz, J. Opt. Soc. Am. B **18**, 1922 (2001).

[28] D. Hansen and A. Hemmerich, Phys. Rev. A **72**, 022502 (2005).
[29] S. Kobayashi, Y. Yamamoto, M. Ito, and T. Kimura, IEEE. J. Quantum. Elect. **18**, 582 (1982).
[30] R. Balhorn, H. Kunzmann, and F. Lebowsky, Appl. Opt. **11**, 742 (1972).
[31] W. H. King, J. Opt. Soc. Am. **53**, 638 (1963).
[32] K. Heilig and A. Steudel, At. Data Nucl. Data Tables **14**, 613 (1974).
[33] C. W. P. Palmer, P. E. Baird, S. A. Blundell, J. R. Brandenberger, C. J. Foot, D. N. Stacey, and G. K. Woodgate, J. Phys. B: At. Mol. Phys. **17**, 2197 (1984).
[34] W. Nortershauser, N. Trautmann, K. Wendt, and B. A. Bushaw, Spectrochim. Acta, Part B **53**, 709 (1998).